Analysis of Integrated Vapor Transport Biases

CAROLYN A. REYNOLDS,[a] WILLIAM CRAWFORD,[a] ANDREW HUANG,[b] NEIL BARTON,[a] MATTHEW A. JANIGA,[a] JUSTIN MCLAY,[a] MARIA FLATAU,[a] SERGEY FROLOV,[a] AND CLARK ROWLEY[c]

[a] *Marine Meteorology Division, U. S. Naval Research Laboratory, Monterey, California*
[b] *Science Applications International Corporation, Monterey, California*
[c] *Ocean Sciences Division, U. S. Naval Research Laboratory, Stennis Space Center, Mississippi*

(Manuscript received 26 July 2021, in final form 21 January 2022)

ABSTRACT: High-fidelity analyses and forecasts of integrated vapor transport (VT) are central to the study of Earth's hydrological cycle as well as high-impact phenomena such as monsoons and atmospheric rivers. The impact of the in-line analysis correction-based additive inflation (ACAI) on IVT biases and forecast errors is examined within the Navy Earth System Prediction Capability (Navy ESPC) global coupled system. The ACAI technique uses atmospheric analysis corrections from the data assimilation system to approximate model bias and as a representation of stochastic model error to simultaneously reduce systematic and random errors and improve ensemble performance. ACAI reduces the global average magnitude of the 7- and 14-day IVT bias by 16%–17% during Northern Hemisphere summer, reaching 70% reductions in some tropical regions. The global average IVT bias reduction is similar to the bias reduction for low-level wind speed bias and considerably smaller than the bias reduction in total precipitable water. The localized regions where ACAI increases IVT bias occur where the control IVT biases change sign and structure with increasing forecast lead time, such as the South Asian monsoon region. Substituting analyzed wind or moisture fields for the forecast fields when calculating the forecast IVT confirms that, on average, wind errors dominate the IVT error calculation in the tropics, although wind and moisture error contributions are comparable in the extratropics. The existence of regions where using either analyzed winds or analyzed moisture increases IVT bias or mean absolute error reveals areas with compensating errors.

KEYWORDS: Atmospheric river; Monsoons; Coupled models; Ensembles; Model errors; Numerical weather prediction/forecasting

1. Introduction

The horizontal transport of moisture in the atmosphere, integrated vapor transport (IVT), is central to the concept and study of Earth's hydrological cycle as well as high-impact phenomena such as monsoons and atmospheric rivers (ARs). IVT and related quantities are used, for example, to analyze the global energy and hydrological cycles (e.g., Peixoto and Oort 1992; Trenberth et al. 2011), meridional latent heat transport in the general circulation (e.g., Shaw and Pauluis 2012), moisture flux convergence in El Niño precipitation anomalies (Mo and Higgins 1996), decadal trends in tropical circulations (Sohn and Park 2010), and the west African Monsoon (WAM) cycle and variability (Thorncroft et al. 2011; Lélé et al. 2015). IVT is also used to define ARs (Shields et al. 2018; Rutz et al. 2019; Ralph et al. 2019). ARs are long filaments of horizontal moisture vapor transport (Zhu and Newell 1998; Ralph et al. 2017; Gimeno et al. 2014) that are associated with both beneficial and hazardous impacts (e.g., Ralph et al. 2006; Dettinger et al. 2011; Lavers et al. 2011; Neiman et al. 2011; Ramos et al. 2015).

Given the central role that IVT plays in these high-impact phenomena, previous studies investigate model errors and biases in simulating and forecasting IVT and its wind and moisture components on a range of time scales and applications. In a comparison of the National Centers for Environmental Prediction (NCEP) and NASA Data Assimilation Office (DAO) reanalyses, discrepancies in tropical moisture transport are largely due to differences in the divergent wind (Mo and Higgins 1996). Humidity contributes more than wind to IVT differences between the European Centre for Medium-range Weather Forecasts (ECMWF) Reanalysis version 5 (ERA5; Hersbach et al. 2020) and AR reconnaissance (Ralph et al. 2020) dropsondes above 800 hPa, while winds contribute more than humidity at lower levels (Cobb et al. 2021). Examination of the ECMWF Integrated Forecast System (IFS) shows that the largest contributor to northeastern Pacific IVT uncertainty in analyses and short forecasts is 850-hPa winds, and that dry biases and low wind speed biases contribute to a low bias in water vapor flux (Lavers et al. 2018, 2020). Nardi et al. (2018) find IVT bias of over 15% over portions of the northeastern Pacific over the first 3 days of the forecast when both forecast and verifying analysis had a strong AR (with IVT $>$ 500 kg m^{-1} s^{-1}). Studies have also looked at moisture transport errors in monsoon regions, with the WAM receiving considerable attention as part of the

Supplemental information related to this paper is available at the Journals Online website: https://doi.org/10.1175/MWR-D-21-0198.s1.

Huang's current affiliation: Core Logic, Boulder, Colorado.

Frolov's current affiliation: NOAA/Physical Science Laboratory, Boulder, Colorado.

Corresponding author: Carolyn Reynolds, carolyn.reynolds@nrlmry.navy.mil

DOI: 10.1175/MWR-D-21-0198.1

African Monsoon Multidisciplinary Analysis (AMMA; Redelsperger et al. 2006). In an intercomparison of water budgets from ECMWF Interim reanalyses and NCEP Reanalysis I and II, Meynadier et al. (2010) use operational forecast models to show that significant biases in the Saharan heat low–driven meridional circulations contribute to errors in the representation of the WAM water cycle. In general circulation model seasonal forecasts there are substantial biases and inter-model differences in the 900-hPa moisture fluxes and winds associated with the June–September WAM (Xue et al. 2010). Likewise, moisture flux over the western Indian Ocean is shown to contribute to the precipitation deficits in NCEP coupled forecast system model version 2 (CFSv2) Indian monsoon simulations (Sahana et al. 2019).

Forecast errors in IVT and other fields are due to initial state and model errors, and an ensemble forecast system that accounts for model uncertainty can result in improved probabilistic forecasts and reduced forecast biases on many different time scales (Berner et al. 2017). Improved stochastic forcing in the NCEP Global Ensemble Forecast System (GEFS) increases the extent of skillful forecast lead times by about 4 days (Li et al. 2019). The new stochastic forcing has a significant impact on both the amplitude and phase errors of the MJO. The new schemes also reduce the model forecast biases in tropical zonal winds, temperature, and humidity. Stochastically perturbed parameterization tendencies (SPPTs) improve the ECMWF seasonal forecasting system through reducing overly strong convection in the Maritime Continent area, in turn reducing biases in outgoing longwave radiation (OLR), cloud cover, precipitation, and lower-tropospheric winds (Weisheimer et al. 2014). There is also an improvement in the realism of the frequency and amplitude of the MJO. Given these previous results, we may expect that accounting for model uncertainty in an ensemble system will likewise improve forecasts of IVT.

Crawford et al. (2020) evaluate the impact of analysis correction-based additive inflation (ACAI) on the performance of the uncoupled Navy Global Environmental Model (NAVGEM) for a variety of deterministic and ensemble metrics. The in-line ACAI method, based on the earlier work of Piccolo and Cullen (2016), Bowler et al. (2017) and Piccolo et al. (2019), has both a systematic component (here constructed from a seasonal mean) and a random component, and is designed to both correct model biases and enhance ensemble spread. In the uncoupled system study of Crawford et al. (2020), the addition of ACAI improves bias and RMSE for lower-tropospheric temperature and 500-hPa height, although ACAI leads to a degradation of some biases at long lead times. ACAI also improves the match between squared ensemble spread and the bias-corrected ensemble mean squared error (or ensemble calibration) in an ensemble formulation in which the initial perturbations are produced using an ensemble of data assimilation (EDA) method.

Given how central IVT is to the general circulation and hydrological cycles and certain types of high-impact weather, such as monsoons and ARs, and given the success of stochastic methods in improving forecasts, here we evaluate the impact of ACAI on IVT forecasts using the new Navy Earth System Prediction Capability (Navy ESPC; Barton et al. 2021) global coupled system. As IVT has both a wind and moisture component, we use an evaluation of the impact of ACAI on these individual components to understand the impact of ACAI on IVT. To confirm hypotheses based on this component analysis, we use a technique following Camargo et al. (2007), Lavers et al. (2018), and Cobb et al. (2021) in which we recalculate IVT forecast bias and error substituting in reanalysis winds or moisture for the forecast fields to quantify the impacts of each component on IVT biases and errors.

The methodology, including a description of the forecast system, ensemble design, and experimental design, is presented in section 2. The results described in section 3 include an analysis of the impact of ACAI on the prediction of IVT and an analysis of the wind and moisture components of the IVT errors. A brief summary and conclusions are presented in section 4.

2. Methodology

a. *Forecast system*

The Navy ESPC (Barton et al. 2021) is the U.S. Navy's first global coupled forecast system, which became operational at the Fleet Numerical Meteorology and Oceanography Center in August 2020. The system comprises NAVGEM (Hogan et al. 2014) for the atmosphere and the Global Ocean Forecasting System version 3.1 (GOFS 3.1; Metzger et al. 2014) for the ocean and cryosphere. GOFS comprises the Hybrid Coordinate Ocean Model (HYCOM; Chassignet et al. 2003) and the Los Alamos–developed Community ICE model (CICE; Hunke and Lipscomb 2015). The system is coupled using the Earth System Modeling Framework (ESMF; Theurich et al. 2016), using a 1-h coupling time step. The system currently uses a loosely coupled data assimilation (DA) methodology in which the NAVGEM and GOFS systems are initialized with increments from their own data assimilation systems, but use the Navy ESPC coupled forecast for the model background information. For NAVGEM, the DA system is the Naval Research Laboratory (NRL) Atmospheric Variational Data Assimilation System Accelerated Representer (NAVDAS-AR), a hybrid four-dimensional variational system (Rosmond and Xu 2006; Kuhl et al. 2013). GOFS is initialized through the Navy Coupled Ocean Data Assimilation (NCODA) system, a full three-dimensional multivariate DA system (Cummings and Smedstad 2014). The NAVGEM resolution is T359 (approximately 37 km) with 60 levels. In the operational configuration, HYCOM and CICE are run at 1/12° resolution, but in order to save computational resources, the ensemble forecasts examined here use 1/4° resolution in HYCOM with 41 layers and 1/4° CICE with four ice categories. Another difference from the operational configuration is that in these experiments, CICE version 5 is used, while in the operational configuration, CICE version 4 is used. Differences in the configuration of the experimental setup used here and that of the operational system are provided to the reader primarily for the sake of reference. While evaluation of different model configurations do show marginal impacts on the skill of the forecasts, we do not anticipate any dependence of the findings presented here on these

system formulation differences, as the settings and model versions are consistent for all experiments discussed here. For an in-depth description of the Navy ESPC system see Barton et al. (2021), Barton et al. (2019), and Ruston et al. (2019).

b. Ensemble design

Initial perturbations are created using an EDA (Houtekamer et al. 1996; Kucukkaraca and Fisher 2006), i.e., adding random errors to the observations, consistent with observation error statistics, in both NCODA and NAVDAS-AR data assimilation update cycles. Sixteen parallel update cycles are run, with member 0 using the unperturbed observations, and the remaining 15 members using observations with independent random perturbations. These perturbed initial conditions are created using the operational version of Navy ESPC with 1/12° HYCOM and CICE, which are then truncated to the 1/4° resolution for the ensembles considered here. The 16-member 45-day ensemble forecasts are produced once per week (every Wednesday) from 1 February 2017 to 24 January 2018 (a total of 52 ensemble forecasts), although for a fair comparison with other experiments, only 7 of the 16 ensemble forecasts are considered here. Members 1–7 have been selected from the 16 available members in the CTL experiment. As each perturbed member differs only by the specific noise added to the observations in the EDA, there is no expected dependence of the results on the sub-selection of members. These control (CTRL) ensembles are produced without using any methods that account for model uncertainty.

ACAI has been tested in the stand-alone NAVGEM system (Crawford et al. 2020) and is currently being tested in Navy ESPC as a way to decrease model bias, increase ensemble spread, and improve forecast performance. The ACAI perturbations are created from the atmospheric component of the Navy ESPC loosely coupled update cycle from a prior year (2011). This may be suboptimal as the model biases may be a function of the large-scale environmental initial conditions (e.g., ENSO phase), and tests are ongoing to use analysis increments from an update cycle that immediately precedes the forecasts. The in-line ACAI perturbations are added to the atmospheric forecast tendencies as they are integrated forward in time and include both a mean (systematic) and random (stochastic) component taken from an archive of analysis increments. In our current experimental design, the ACAI increments are not added to the short forecasts used in the data assimilation update cycle, such that the initial states for the ACAI and control ensemble forecasts are identical. As mentioned in the introduction, in tests with uncoupled NAVGEM, Crawford et al. (2020) demonstrate significant improvements in both model bias and ensemble mean RMSE overall, although there are some degradations in bias at later lead times. ESPC ensemble forecasts are repeated with the addition of ACAI during the forecast integration, and these forecasts are referred to as ACAI. For computational reasons, the ACAI ensembles contain only seven members, so, as mentioned above, only seven members of the CTL ensemble are considered here for a fair comparison.

c. Diagnostics

IVT is defined as

$$\mathrm{IVT} = -\frac{1}{g}\int_{1000}^{300} qV\,dp, \tag{1}$$

where g is gravity, q is specific humidity, V is wind velocity, and p is pressure. We integrate IVT from 1000 to 300 hPa. Errors in IVT can come from both errors in moisture and errors in wind. We therefore examine errors in total precipitable water (TPW) and low-level winds. In our diagnostics, we focus on bias, but also consider mean absolute error (MAE). Both biases and MAE are calculated for the forecast ensemble means.

For verification, we use the ERA5 global reanalysis (Hersbach et al. 2020). We also use this data to diagnose the relative importance of winds and moisture to IVT biases. For example, to examine the influence of winds on IVT biases, we compute IVT in Eq. (1) using humidity from the ERA5 verifying analysis and winds from our model forecast experiments (CTL_ERAMOIST and ACAI_ERAMOIST). Conversely, to examine the influence of moisture on IVT biases, we use winds from ERA5 and specific humidity from our model forecast in the IVT calculation (CTL_ERAWIND and ACAI_ERAWIND). This diagnostic method follows that of Camargo et al. (2007) in which they use a genesis potential index to diagnose the effects of ENSO on tropical cyclone genesis. They assess the importance of four individual variables that comprise the genesis potential index by using long-term climatological values for three of the genesis potential variables, and interannually varying values for the other variable. Lavers et al. (2018) use a similar diagnostic technique in which they assess the impact of IVT analysis and forecast uncertainty in the ECMWF IFS by substituting in specific humidity or winds in the lower troposphere with unperturbed analysis values or observations using AR Reconnaissance dropsondes in the eastern North Pacific. They find that the 850-hPa winds are the dominant contribution to IVT forecast uncertainty in the analysis and at the 48- and 96-h forecast times. Cobb et al. (2021) also use this technique of substituting in AR Reconnaissance dropwindsonde observations of winds or moisture in the vapor transport calculation in the representation of AR conditions in three reanalyses. They find that humidity differences contribute more than wind differences to moisture transport biases above 800 hPa, while winds dominate at lower levels. While biases do exist in the ERA5 reanalysis IVT (Cobb et al. 2021), they are small (on average less than 13 kg m^{-1} s^{-1}) as compared to the 7- and 14-day forecast errors in this study, so it is reasonable to use the ERA5 reanalysis for verification. In a similar manner, our substitution of the ERA5 moisture or ERA5 winds into the error calculations will allow us to determine the relative contributions of wind and moisture errors to IVT error. We emphasize that this technique specifically identifies the contributions of the wind and moisture errors to the instantaneous calculated IVT errors, not sources of that error. Likely sources of model error, such as the parameterization of deep convection, will result in related errors in the winds, moisture, and temperature fields. The different experiments and IVT component attribution analyses using

TABLE 1. Configuration of the ensemble experiments and diagnostic calculations.

	Model uncertainty	Winds used in error calculations	Specific humidity used in error calculations
CTL	None	Navy ESPC	Navy ESPC
CTL_ERAMOIST	None	Navy ESPC	ERA5
CTL_ERAWIND	None	ERA5	Navy ESPC
ACAI	ACAI	Navy ESPC	Navy ESPC
ACAI_ERAMOIST	ACAI	Navy ESPC	ERA5
ACAI_ERAWIND	ACAI	ERA5	Navy ESPC

ERA5 data substituted for forecast fields are summarized in Table 1.

3. Results

a. *Impact of ACAI on IVT and component biases*

ACAI results in a decrease in the globally averaged magnitude (absolute value) of the IVT ensemble mean bias at all leads times for all seasons, but the reduction is largest for JJA (Fig. 1). These results are consistent with the general bias reductions noted by ACAI in atmosphere-only tests with NAVGEM (Crawford et al. 2020). The biases reach approximate saturation values from around 10 days to 2 weeks into the forecast, when ACAI reduces the global average control bias by 16.4%, 12.8%, 11.2% and 12.6% during JJA, SON, DJF, and MAM, respectively. At forecast day 7, the reductions are 17.7%, 10.3%, 9.5%, and 11.4% for JJA, SON, DJF, and MAM, respectively.

The magnitude and sign of the JJA 14-day IVT biases show considerable spatial variability (Fig. 2a). The largest negative IVT biases occur over the tropical Atlantic, Arabian Sea, and Bay of Bengal. The largest positive biases are over the western-central tropical Pacific and over the Sahel and western Africa just north of the equator in the WAM region, and the Indian Ocean just south of the equator. ACAI generally reduces the magnitude of these biases, as illustrated by a reduction in the saturation of the colors over most regions in Fig. 2b as compared to Fig. 2a. Figure 2c shows the absolute value of the CTL IVT biases subtracted from the absolute value of the ACAI

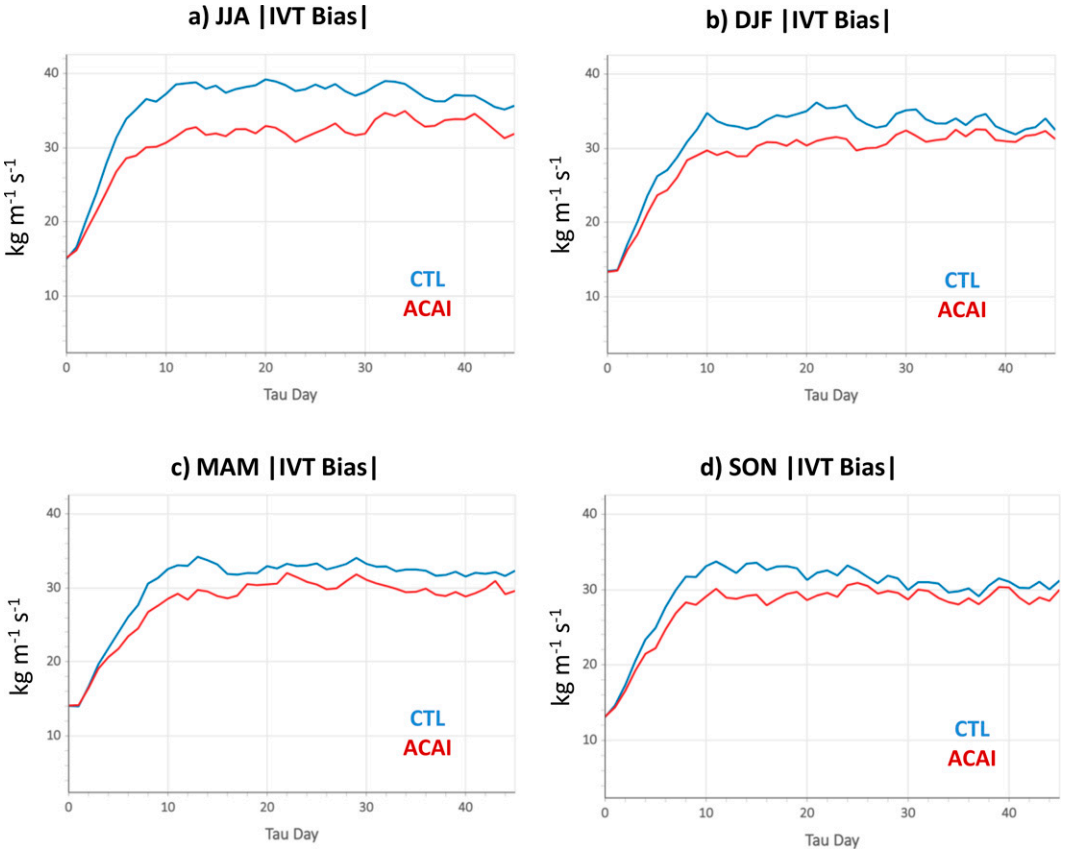

FIG. 1. Global average of the magnitude of the IVT bias (kg m^{-1} s^{-1}) for CTL (blue) and ACAI (red) for (a) JJA, (b) DJF, (c) MAM, and (d) SON as a function of forecast lead time.

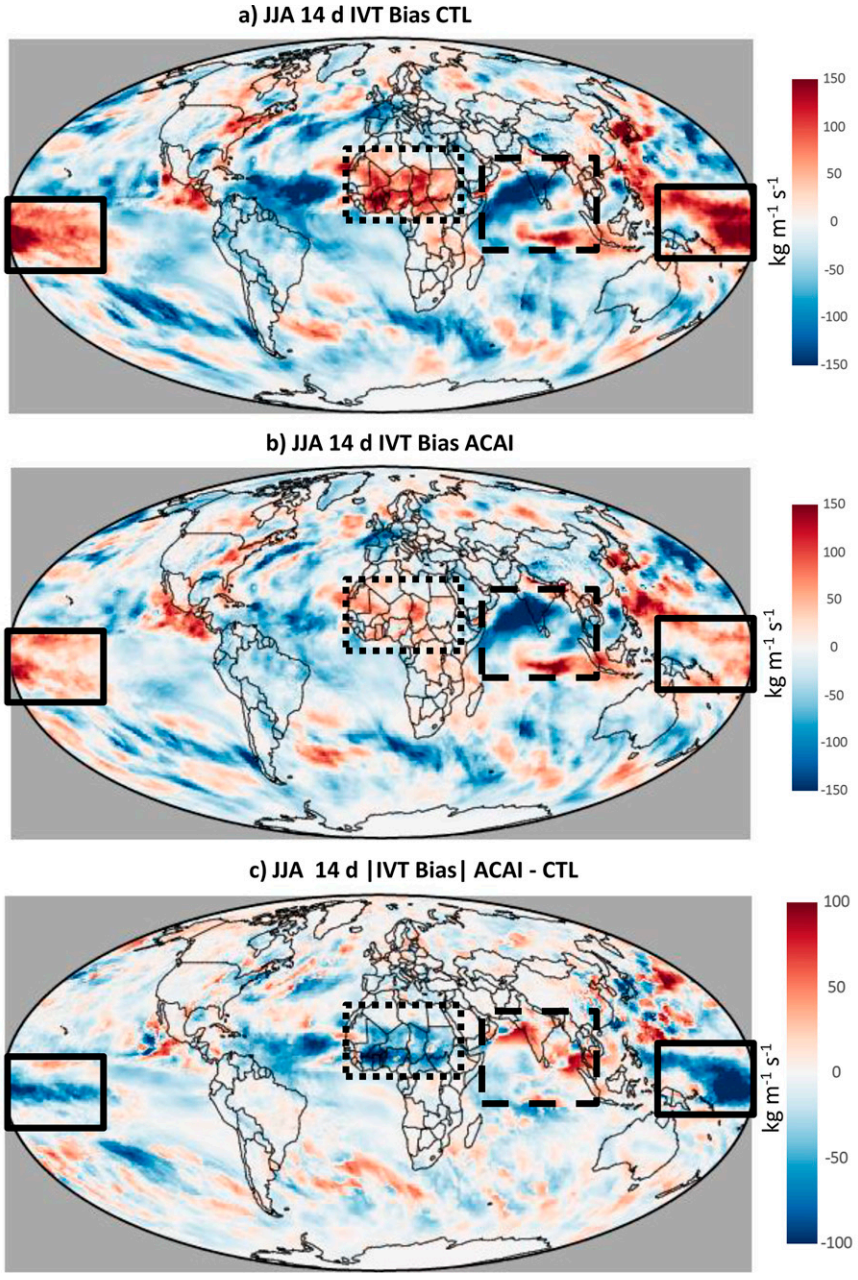

FIG. 2. JJA IVT bias (kg m^{-1} s^{-1}) for (a) CTL, (b) ACAI, and (c) the absolute value of the IVT bias for ACAI minus the absolute value of the IVT bias for CTL (kg m^{-1} s^{-1}) for forecast day 14. The solid, dotted, and dashed boxes denote the western and central tropical Pacific, Indian Ocean, and northern tropical and subtropical African regions referred to in the text.

IVT biases; cool colors indicate regions where ACAI reduces the magnitude of the bias and warm colors indicate regions where ACAI increases the magnitude of the bias. ACAI is particularly effective at reducing biases in the western-central Pacific, the Atlantic, and the WAM region, where significant biases in vapor transport have been identified in other systems as well (e.g., Meynadier et al. 2010; Xue et al. 2010). In some regions of the tropical Pacific and over Africa just north of the Gulf of Guinea, ACAI reduces IVT biases by up to 70%. However, there are some regions, including central Indian and the northern Arabian Sea, and the eastern Bay of Bengal, in the South Asian summer monsoon region, where ACAI increases the IVT bias. Precipitation biases may result from coupled processes and SST cold biases (Wang et al. 2018) and therefore ACAI in the atmosphere may not be sufficient to address them. Some of the

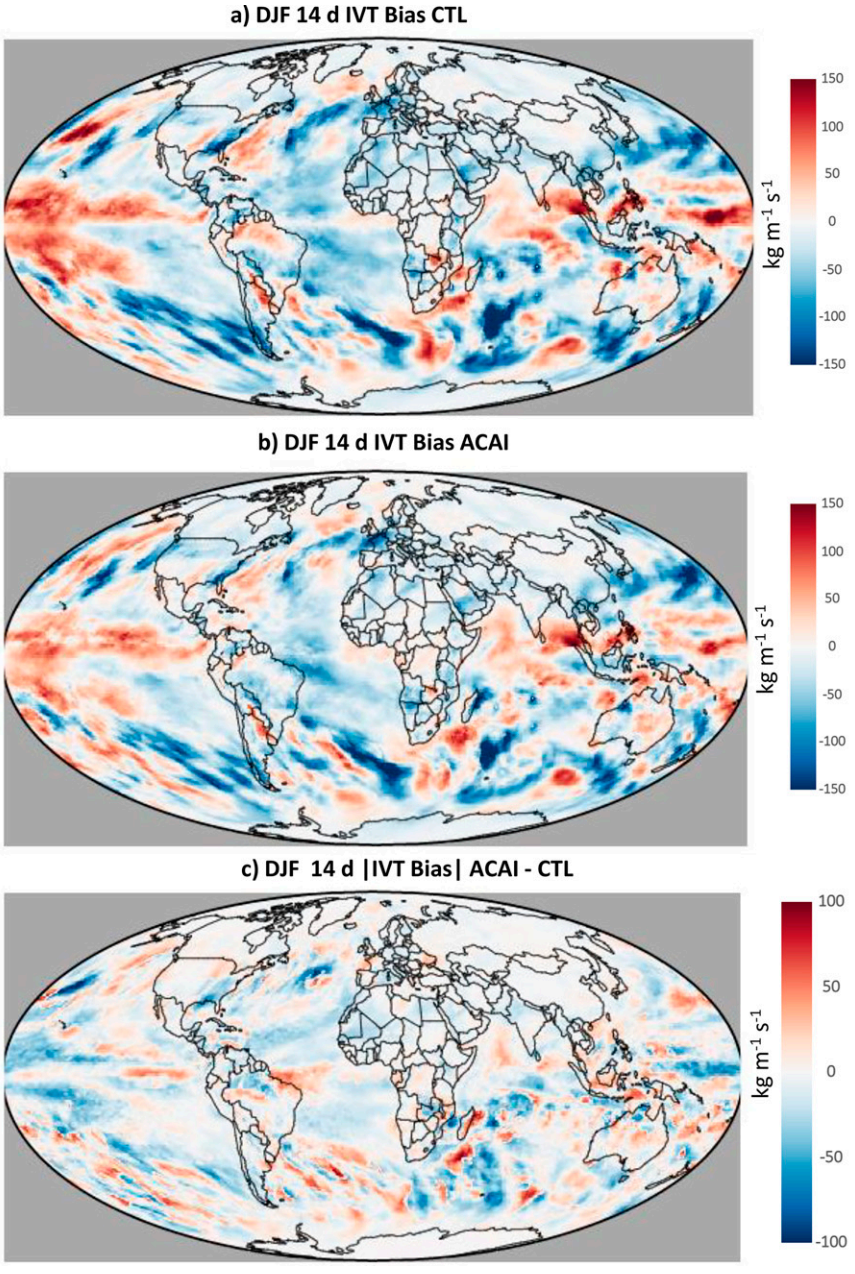

FIG. 3. As in Fig. 2, but for DJF.

noisy patterns in the midlatitudes, particularly over the Southern Ocean and extratropical western Pacific, probably indicate that the relatively small sample size and smaller bias to variance ratio result in the biases being ill defined. Synoptic eddies play a relatively larger role in the meridional transport of moisture in the extratropical storm tracks than in tropical and subtropical regions (Newman et al. 2012), and this is consistent with sampling issues limiting the effectiveness of ACAI in the storm track regions more than in the tropics.

The large JJA IVT over western Africa and the Arabian Sea and India, associated with the WAM and South Asian Monsoon (Fig. 2), are replaced by much smaller biases during DJF in those regions (Fig. 3), when the boreal summer monsoon is no longer active. The IVT biases in regions associated with the boreal winter monsoon, such as northern Australia, southern Africa and southern Brazil, are weaker and not as spatially coherent as those associated with the boreal summer monsoon. There is still a positive IVT bias over the tropical western and central Pacific, but the bias itself, as well as the

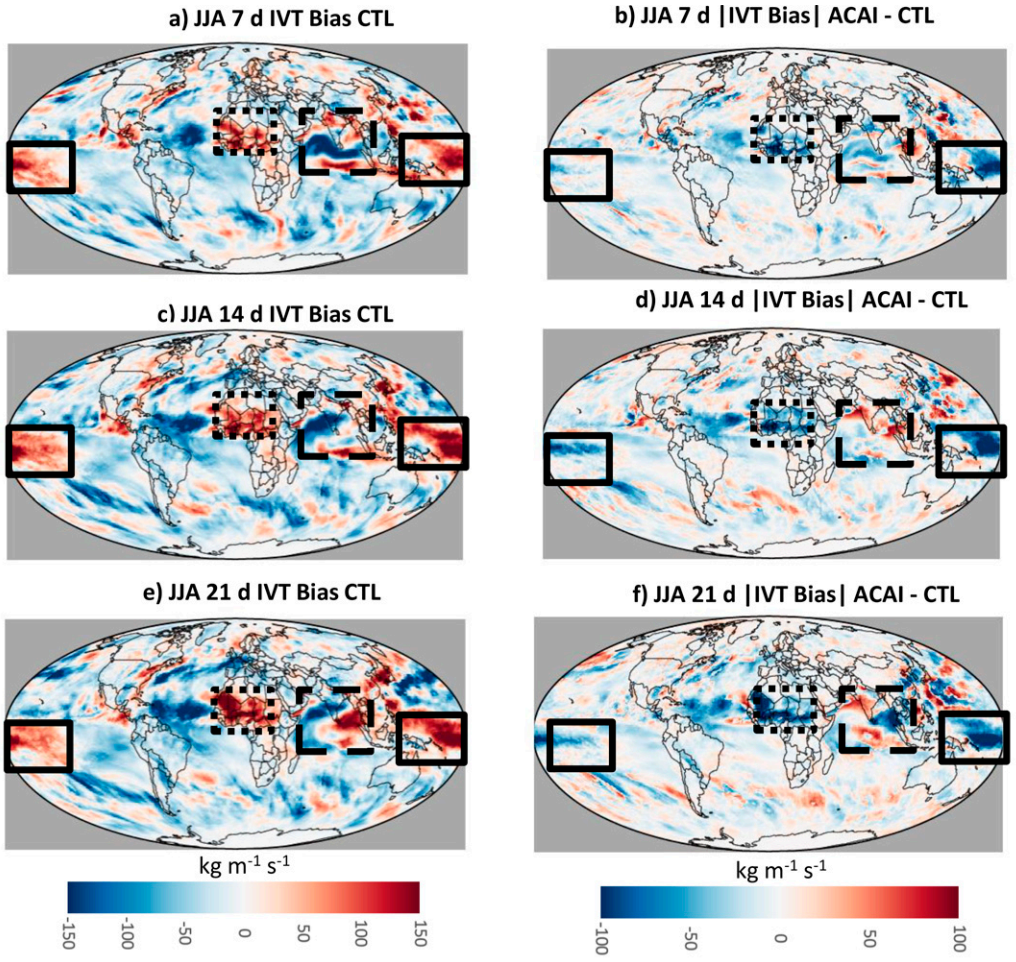

FIG. 4. (left) JJA IVT bias (kg m^{-1} s^{-1}) for CTL and (right) the absolute value of the ACAI IVT bias minus the absolute value of the CTL IVT bias (kg m^{-1} s^{-1}) for forecast days (a),(b) 7; (c),(d) 14; and (e),(f) 21. Panels (c) and (d) are the same as Figs. 2a and 2c and are repeated to facilitate comparison. The solid, dotted, and dashed boxes denote the western and central tropical Pacific, Indian Ocean, and northern tropical and subtropical African regions referred to in the text.

ACAI correction of the bias, are smaller in DJF than in JJA. Because the biases and the IVT corrections are largest in the tropics during JJA, we focus on tropical regions during this season when interpreting ACAI's impact. However, for the sake of completeness, we include the results for other seasons in the supplemental figures (Figs. S1–S6).

As described in Crawford et al. (2020), the systematic component of ACAI based on a time average of analysis increments is designed to counteract model biases (although the stochastic component is also effective at reducing biases). The design of ACAI is based on the concept that the short-term biases diagnosed in the update cycle are representative of the model biases that develop later in the forecast integration and that bias characteristics remain similar through the forecast integration time. Maps of the 7-, 14-, and 21-day IVT biases (Figs. 4a,c,e) indicate that in general the bias patterns remain similar during the integration time, particularly for the large biases over the western-central tropical Pacific, tropical Atlantic, and WAM region. This tendency for many model systematic errors to stabilize early in the forecast, especially those associated with convection, is also found in other models (e.g., Xie et al. 2012). These are regions where ACAI is particularly effective at reducing biases at all three forecast times (Figs. 4b,d,f). In contrast, over regions where the IVT bias changes with time, such as over India and the Bay of Bengal, ACAI does not reduce the biases at all lead times. The band of weak IVT bias over the Arabian Sea moves northward in time, which may indicate that this particular bias is associated with the evolution of the South Asian monsoon, or perhaps with the boreal summer intraseasonal oscillation (BSISO; Lawrence and Webster 2002; Lee et al. 2013). The inability for analysis increment-based correction schemes to represent state-dependent error statistics is noted in Piccolo et al. (2019) as a potential reason that these schemes may increase ensemble mean RMSE for some fields, despite overall promising performance.

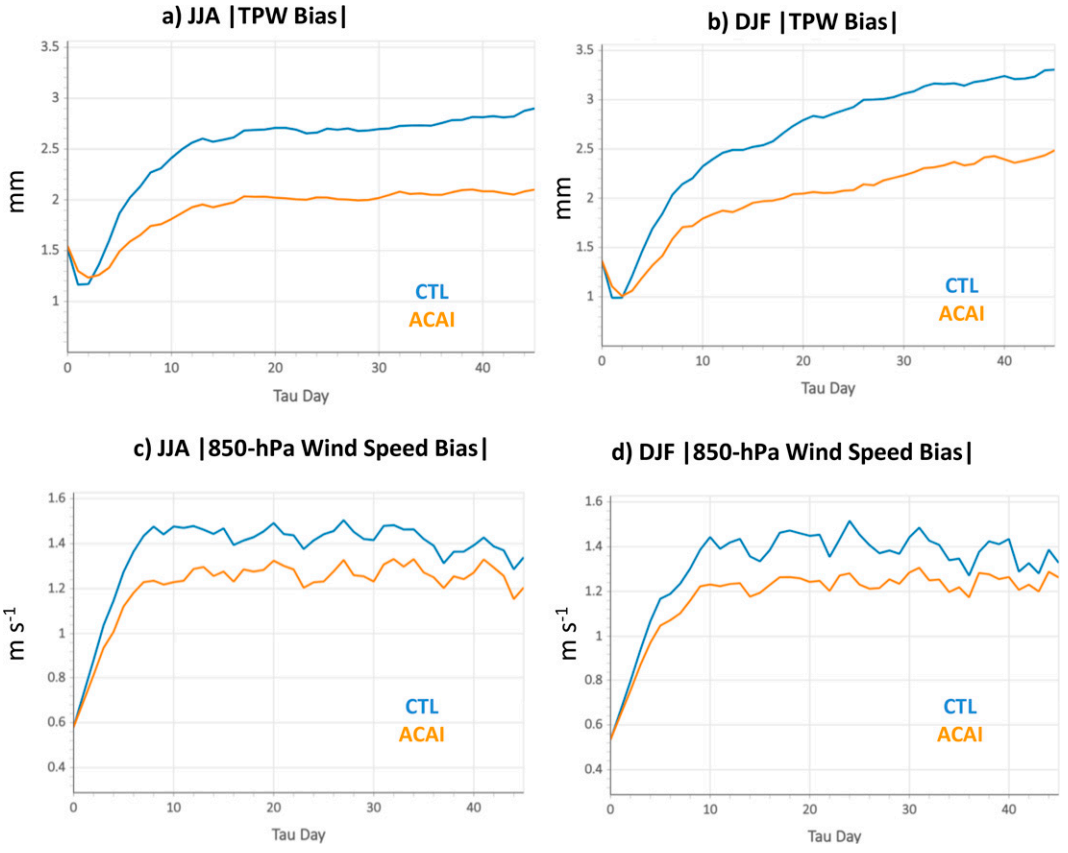

FIG. 5. (a),(b) Global average bias magnitude for CTL (blue) and ACAI (orange) for TPW (mm) and (c),(d) 850-hPa wind speed (m s^{-1}) for (left) JJA and (right) DJF as a function of forecast lead time in days.

As both wind and moisture biases and errors may contribute to IVT biases and errors, we consider the impact of ACAI on TPW and 850-hPa wind speed separately (Fig. 5). We focus on the 850-hPa level for the winds based on the Lavers et al. (2018) result that the winds at that level contribute more to 2- and 4-day forecast uncertainty in IVT than winds at 925 or 700 hPa. Preliminary analysis indicated that the results for winds at the 925-hPa level were very similar. ACAI is very effective at reducing the TPW bias (by 29.1% and 28.3% at forecast day 7 for JJA and DJF, respectively, and by 33.2% and 31.1% at forecast day 14 for JJA and DJF, respectively). ACAI also reduces 850-hPa wind speed biases, but the percent reduction is about half of that for the TPW bias reduction (by 16.3% and 14.5% at forecast day 7 for JJA and DJF, respectively, and by 14.3% and 15.3% at forecast day 14 for JJA and DJF, respectively). TPW bias reductions in MAM are similar to JJA and those in SON are similar to DJF, while the wind speed bias reductions are smaller in MAM and SON than in JJA or DJF (Fig. S1). The larger impact of ACAI on TPW than on low-level wind speed is also apparent in the maps of the 14-day biases (Fig. 6). ACAI reduces the magnitude of the large TPW biases over the Sahel and most of the subtropics (cf. Figs. 6a,c,e), but results in larger biases in some regions such as the tropical Indian Ocean. ACAI effectively increases TPW over most tropical and subtropical oceanic regions, and this results in a decrease in TPW bias over the regions where CTL is too dry, but can result in an increase in TPW bias over regions where CTL is too moist, such as the near-equatorial Indian Ocean. During DJF (Fig. S2), ACAI is likewise effective at reducing TPW bias over many regions of the tropics, particularly over the tropical Atlantic and southern Indian Ocean, but it results in increased biases in other tropical areas, including the tropical eastern Pacific and the northern Indian Ocean and Bay of Bengal. For 850-hPa wind speed, the impact of ACAI is more mixed, with significant bias reductions over the western Pacific tropical region and northern tropical Africa, but increases in bias over parts of India, the eastern Indian Ocean, and regions of the extratropics. As with the IVT biases, the regions where ACAI has the largest positive impact on wind speed tend to be where the sign of the bias in the CTL forecast stays the same over different lead times (e.g., the western tropical Pacific and northern equatorial Africa, not shown). The regions where ACAI has a negative impact tend to be regions where the CTL bias changes with forecast lead time. As mentioned above, this may be due to the model bias changing with the evolution of the South Asian summer monsoon, or perhaps with the BSISO. ACAI will also be less effective in regions where the model biases are a function of large-scale environmental anomalies (e.g., ENSO),

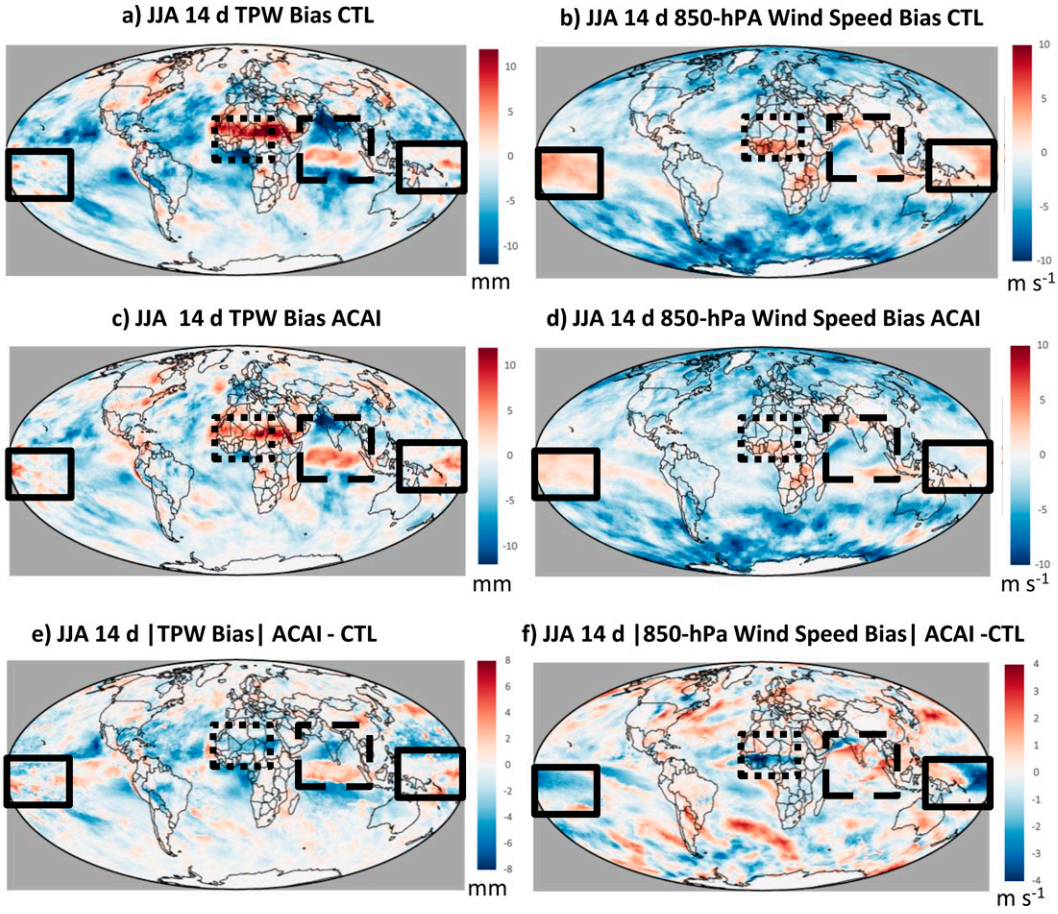

FIG. 6. JJA 14-day TPW bias (mm) for (a) CTL, (c) ACAI, and (e) the absolute value of the TPW bias for ACAI minus the absolute value of the TPW bias for CTL (mm). JJA 14-day 850-hPa wind speed bias (m s^{-1}) for (b) CTL, (d) ACAI, and (f) the absolute value of the wind speed bias for ACAI minus the absolute value of the wind speed bias for CTL (m s^{-1}). The solid, dotted, and dashed boxes denote the western and central tropical Pacific, Indian Ocean, and northern tropical and subtropical African regions referred to in the text.

and where the anomalies differ between the time period used to create the analysis increment archive and the forecast time period.

The percent reduction in IVT bias (Fig. 1) gained through the addition of ACAI is similar to that seen in the percent reduction in wind speed bias (Figs. 5c,d), but substantially smaller than the percent reduction in TPW (Figs. 5a,b), which suggests that winds may be having a bigger impact on IVT biases than moisture. Comparing the 14-day CTL IVT bias (Fig. 2a) with the CTL TPW and CTL 850-hPa wind speed biases (Figs. 6a,b) suggests that the dominant term (either moisture or winds) is regionally dependent. In the western and central tropical Pacific, the positive IVT bias appears related to the positive wind bias, while the TPW bias in that region is less spatially coherent. Over Africa, the positive IVT bias is related to a positive wind speed bias directly north of the Gulf of Guinea, over the Ivory Coast, Ghana, Nigeria, and neighboring countries, in a region where the TPW bias is near zero. Conversely, the positive IVT bias directly north of this region, over the Sahel, corresponds to a region of positive TPW bias, but near neutral to slightly negative wind speed biases.

The impact of ACAI on IVT biases can likewise be interpreted through evaluation of the impact of ACAI on TPW and wind speed biases. The spatial patterns of the impact of ACAI on 14-day IVT biases (Fig. 2c) is more similar to corresponding plots for wind speed (Fig. 6f) than for TPW (Fig. 6e). For example, the large reduction in IVT bias over the tropical western Pacific corresponds to a large reduction in wind speed bias in that region. The same is true for northern equatorial Africa, particularly over Ghana and the Ivory Coast. In both of these regions, ACAI has either a small or slight positive impact on the TPW biases. ACAI also results in an increase in IVT bias over regions of the Arabian Sea and parts of India, and a similar increase is shown for the wind speed biases. Again the Sahel is a contrasting region, where ACAI results in reduced IVT and TPW biases, but has negligible impact on wind speed biases. However, overall, a comparison of IVT biases with wind speed and TPW biases indicates that the wind speed biases dominate IVT biases in most regions. We

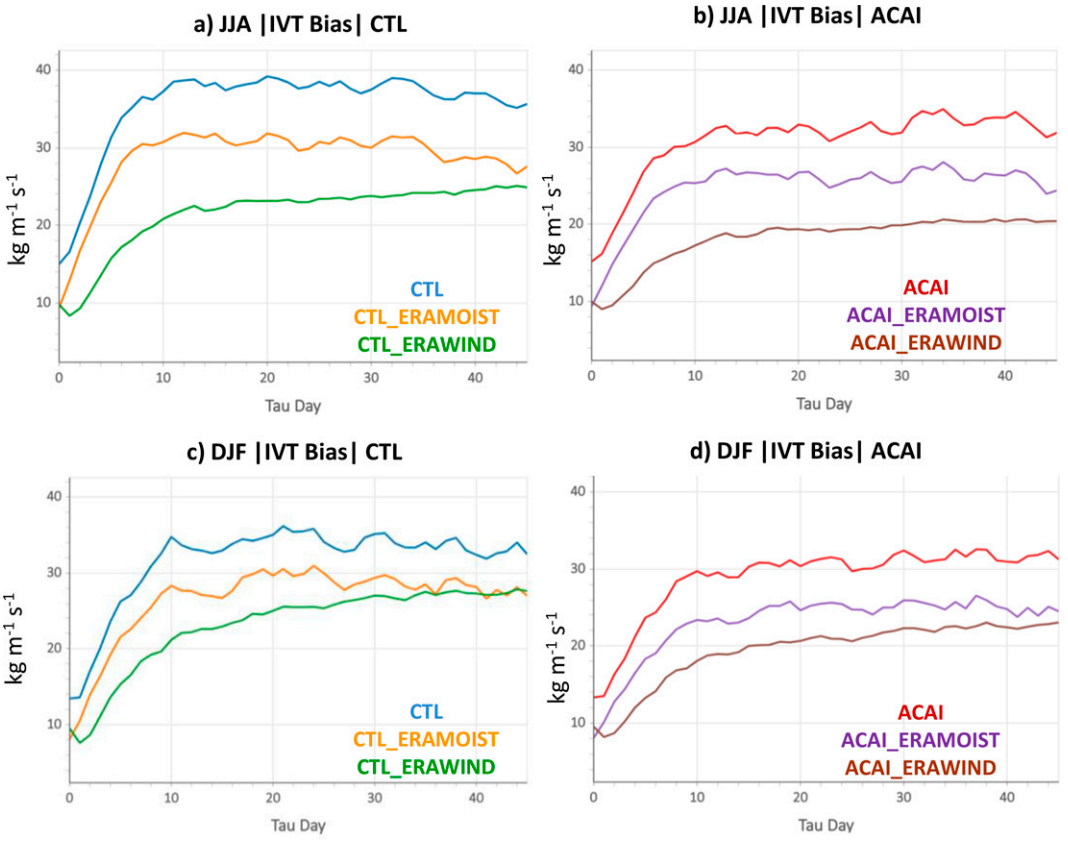

FIG. 7. Global average of the absolute value of the IVT bias (kg m^{-1} s^{-1}) for CTL (blue), CTL_ERAMOIST (gold), and CTL_ERAWIND (green) for (a) JJA and (c) DJF; and for ACAI (red), ACAI_ERAMOIST (purple), and ACAI_ERAWIND (brown) for (b) JJA and (d) DJF as a function of forecast lead time in days.

test this hypothesis directly in the next section where we consider the impact of substituting either analyzed winds or analyzed moisture in the IVT calculation and then recalculating the forecast biases and errors.

b. *Component evaluation of IVT bias and error*

Substituting either ERA5 winds or ERA5 moisture into the IVT calculations confirms that for the global average, the wind errors are the dominant factor in IVT bias calculations for the first month of forecast lead time (Fig. 7). For JJA, substituting in the ERA5 specific humidity while using the forecast winds results in a 17.5% and 16.6% reduction in IVT bias for the 14-day forecasts for CTL and ACAI simulations, respectively (Figs. 7a,b). The percent bias reduction is over twice as large (42.4% and 42.1%) when substituting in the ERA5 winds while using the forecasted moisture. Similar results are found for DJF, where using the ERA5 moisture reduces the 14-day IVT bias by 17.3% for CTL and 20.5% for ACAI, and using the ERA5 winds reduces the bias by 30.7% in CTL and 33.7% in ACAI. The fractional reductions when using the ERA5 winds are even larger for the 7-day IVT bias than the 14-day bias (reaching 48.6% and 36.3% in JJA and DJF, respectively, for the CTL case), although as lead time increases, the impact of using the ERA5 winds is gradually reduced, particularly in the DJF CTL case. The impact of using analyzed winds and analyzed moisture on the IVT biases during SON are very similar to the results for DJF, while the impacts during MAM are qualitatively similar to the results for JJA, but of smaller magnitude (Fig. S3).

The maps of the JJA 14-day IVT bias (Fig. 8) show that the overall magnitude of the impact on the bias is greater when using the ERA5 winds than when using the ERA5 moisture. In the western-central tropical Pacific, the positive IVT bias in CTL (Fig. 8a) remains basically unchanged in CTL_ERAMOIST (Fig. 8b), and the magnitude of the biases in CTL and CTL_ERAMOIST (Fig. 8d) are comparable (slightly increased in some parts of this region). In contrast, CTL_ERAWIND reduces this IVT bias to near zero (Fig. 8c). This confirms the hypotheses developed in the previous section based on the low-level wind speed and moisture biases (Figs. 6a,b) that the IVT biases in this region are primarily due to wind biases. Similar examination of northern tropical and subtropical Africa indicates that CTL_ERAWIND reduces the IVT bias over the whole region, but is particularly effective at reducing the biases in the southern portion of that region, just north of the Gulf of Guinea. CTL_ERAMOIST on the other hand reduces the biases over the Sahel (and actually increases the biases along the coast). This is again consistent with the large positive moisture biases over

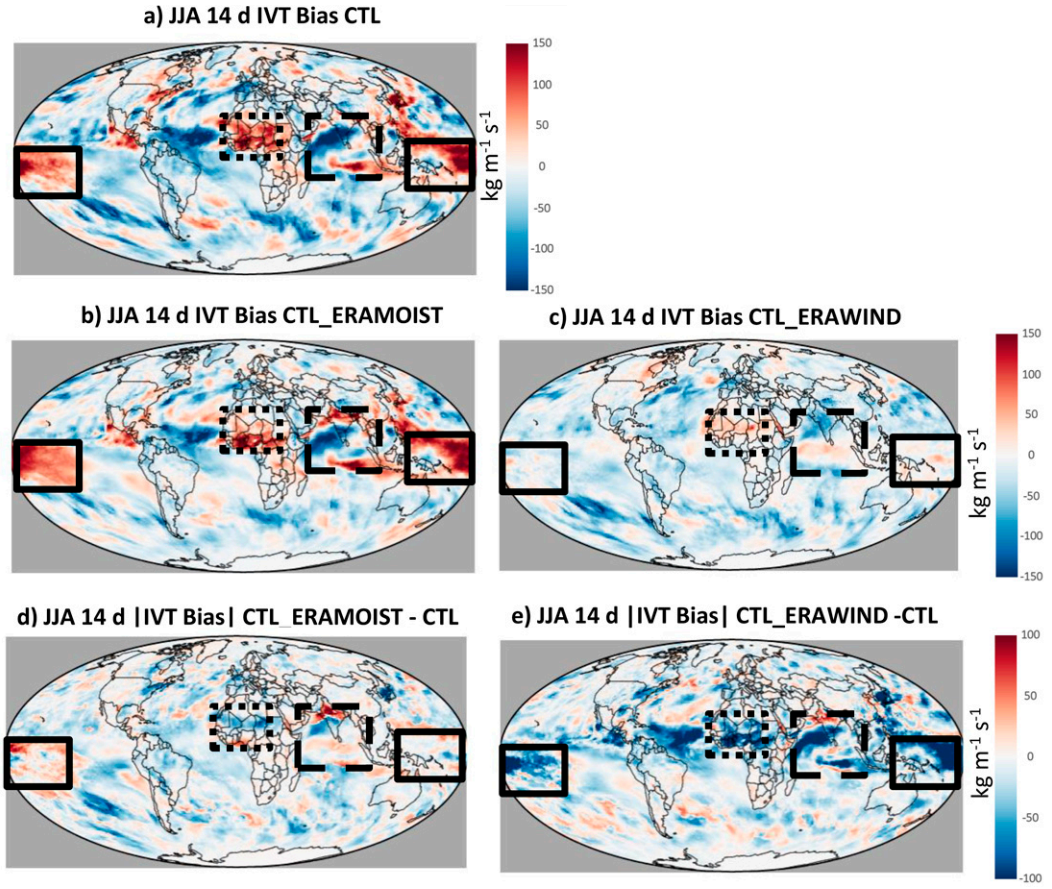

FIG. 8. JJA 14-day IVT bias (kg m^{-1} s^{-1}) for (a) CTL, (b) CTL_ERAMOIST, (c) CTL_ERAWIND, (d) absolute value of CTL bias minus absolute value of CTL_ERAMOIST bias, and (e) absolute value of CTL bias minus absolute value of CTL_ERAWIND bias (kg m^{-1} s^{-1}). The solid, dotted, and dashed boxes denote the western and central tropical Pacific, Indian Ocean, and northern tropical and subtropical African regions referred to in the text.

the Sahel (Fig. 6a), and significant positive wind speed biases immediately north of the Gulf of Guinea (Fig. 6b).

Substituting the analyzed winds or analyzed moisture for the forecast fields does not reduce the IVT bias everywhere, as indicated by the regions with warm colors in Figs. 8d and 8e. This points to compensating errors between the wind and moisture fields. This effect is most pronounced over the extreme northern Bay of Bengal and northern India. The negative moisture biases in the regions (Fig. 6a) are counteracted by the positive wind speed biases (Fig. 6b), such that replacement of either with the analyzed fields actually increases the IVT biases. This also explains why ACAI actually results in an increase of IVT bias in this region (Fig. 2c) despite the fact that ACAI reduces wind biases here (and increases the wind biases just to the south of this region, Fig. 6f) and has a near neutral impact on the dry moisture biases here. Another example is the southern Pacific region off the coast of Peru and Chile. Here the dry bias and the positive wind speed bias compensate each other, such that removal of the bias in either component actually increases the IVT bias. Analogous plots to Fig. 8 for DJF instead of JJA (Fig. S4) likewise show a larger contribution to error reduction by the winds as compared to moisture in most areas, while also showing regions (e.g., the equatorial Atlantic or western Pacific just north of the equator) were compensating errors lead to increased error in IVT when using either analyzed winds or analyzed moisture.

In addition to examining the nature of the IVT biases, we also examine the IVT mean absolute error (MAE) of the ensemble mean. Similar to the bias calculation (Fig. 7), substituting in the ERA5 winds reduces the IVT MAE about twice as much as the reduction obtained by substituting in the ERA moisture (Fig. 9). We separate the CTL and ACAI sets of curves in Fig. 7 because the different sets of curves overlap for the absolute value of the bias, which decreases visual clarity. In contrast, the MAE CTL and ACAI sets of curves do not overlap such that we can include them on the same plot without sacrificing visual clarity in Fig. 9. CTL_ERAWIND and ACAI_ERAWIND MAE is approximately 50% smaller than CTL and ACAI MAE, respectively, during JJA for 7- and 14-day forecasts, (43.3%–45.0% smaller during DJF). The reductions for

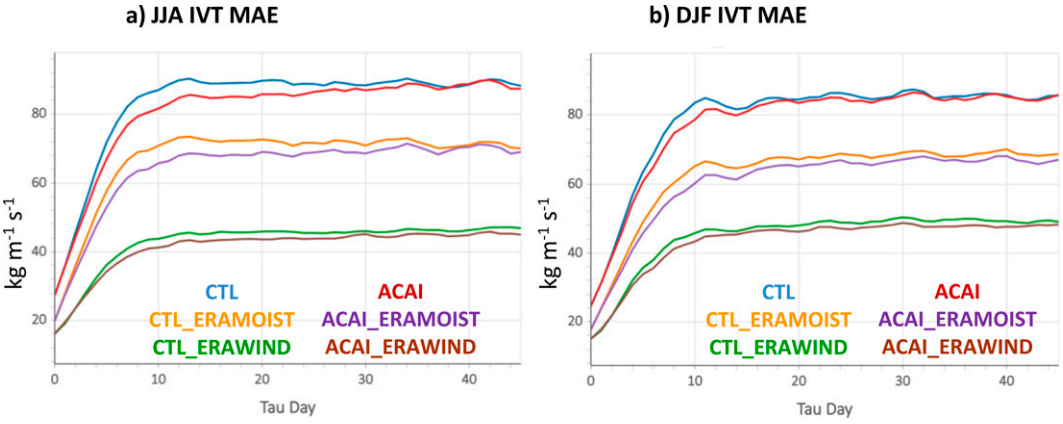

FIG. 9. Global average of the IVT mean absolute error (MAE; kg m^{-1} s^{-1}) for (a) JJA and (b) DJF for CTL (blue), CTL_ERAMOIST (yellow), CTL_ERAWIND (green), ACAI (red) ACAI_ERAMOIST (purple), and ACAI_ERAWIND (brown) as a function of forecast lead time in days.

CTL_ERAMOIST and ACAI_ERAMOIST are between 18.5% and 20.1% for JJA and between 18.1% and 25.5% for DJF. Note that ACAI also reduces the MAE (out to 5 weeks for JJA, and out past two weeks in DJF), although the percent reductions (6.5% and 5.7% at day 7 for JJA and DJF, respectively, and 4.6% and 2.2% at day 14 for JJA and DJF, respectively), are considerably smaller than the ACAI-induced reductions to the IVT bias (Fig. 1). Comparable plots for MAM and SON (Fig. S5) show similar results. Maps of the JJA MAE for CTL and CTL_ERAWIND at forecast day 7 (Figs. 10a,d) show that using the ERA5 winds reduces the MAE in all tropical regions to very small values. Using ERA5 winds also reduces the IVT MAE in DJF substantially (Fig. S6), though not to the same degree as is seen during JJA. The reduction in IVT MAE from using ERA5 moisture is smaller than using ERA5 winds (cf. Figs. 10e,f) in the subtropics and tropics. There are some regions where CTL_ERAMOIST has slightly larger MAE than CTL, indicating compensating wind and moisture errors. However, in many extratropical regions, it appears that the moisture and winds make similar contributions to the IVT MAE. This is also true in DJF (Fig. S6), where moisture makes similar or larger contributions to the IVT MAE as compared to the wind errors in both the Southern Hemisphere and Northern Hemisphere storm tracks. The ACAI (Fig. 10b) and CTL (Fig. 10a) MAE values are similar, and the difference between the two (Fig. 10g) indicates that ACAI reduces MAE over many areas of the tropics, while the impact on extratropics is mixed.

The largest biases in IVT in the control simulation, along with the largest impact of ACAI, are mostly in the tropics and subtropics (Fig. 2). The impact of ACAI on the IVT biases in the extratropics are smaller or less spatially cohesive. However, the IVT MAE can be substantial in the storm tracks in both hemispheres in JJA (Fig. 10) and DJF (Fig. S6). Given the impact of ARs in the extratropics from both a hydrological and hazards perspective (e.g., Lavers and Villarini 2013; Albano et al. 2020; Viale et al. 2018), it is of interest to look specifically at IVT errors in the extratropics. Due to the relatively small sample size, particularly in the storm track regions where a substantial amount of meridional vapor transport is associated with synoptic scale variability (Newman et al. 2012), we consider the bias reduction over the full year, rather than breaking the results down by season.

CTL_ERAMOIST and CTL_ERAWIND result in substantial reductions in 7-day forecast MAE over the storm tracks in both the Northern and Southern Hemispheres (Fig. 11). For example, the MAE in CTL and ACAI off the mid-Atlantic region and New England, and just south of the Canadian Maritimes, reaches values above 200 kg m^{-1} s^{-1}. Both CTL_ERAMOIST and CTL_ERAWIND reduce these errors by over 100 kg m^{-1} s^{-1}. In the eastern North Pacific off the U.S. West Coast, the CTL and ACAI MAE values are between 100 and 150 kg m^{-1} s^{-1}. In this region the CTL_ERAMOIST actually results in a larger error reduction than CTL_ERAWIND. This indicates that wind and moisture errors make comparable contributions to the IVT errors in the midlatitudes. A similar situation is found in the Southern Hemisphere, where the error reduction in CTL_ERAMOIST is larger than in CTL_ERAWIND over the South Atlantic and India Ocean storm tracks. This is in contrast to the situation over most tropical and subtropical regions, where the IVT errors are dominated by the wind errors. The impact of ACAI in these extratropical regions on MAE is relatively small, usually less than 30 kg m^{-1} s^{-1}, and spatially noisy, indicating that a larger sample size would be needed to tease out any systematic impacts. To look at the impacts of ACAI specifically on ARs, one would need a larger sample size and should consider cases where IVT is above a certain threshold (e.g., Cordeira and Ralph 2021), or use specific AR forecast skill metrics (e.g., Nardi et al. 2018; DeFlorio et al. 2018; DeFlorio et al. 2019).

4. Summary and conclusions

We examine the impact of an atmospheric in-line bias correction system (ACAI) on the IVT biases in the Navy ESPC

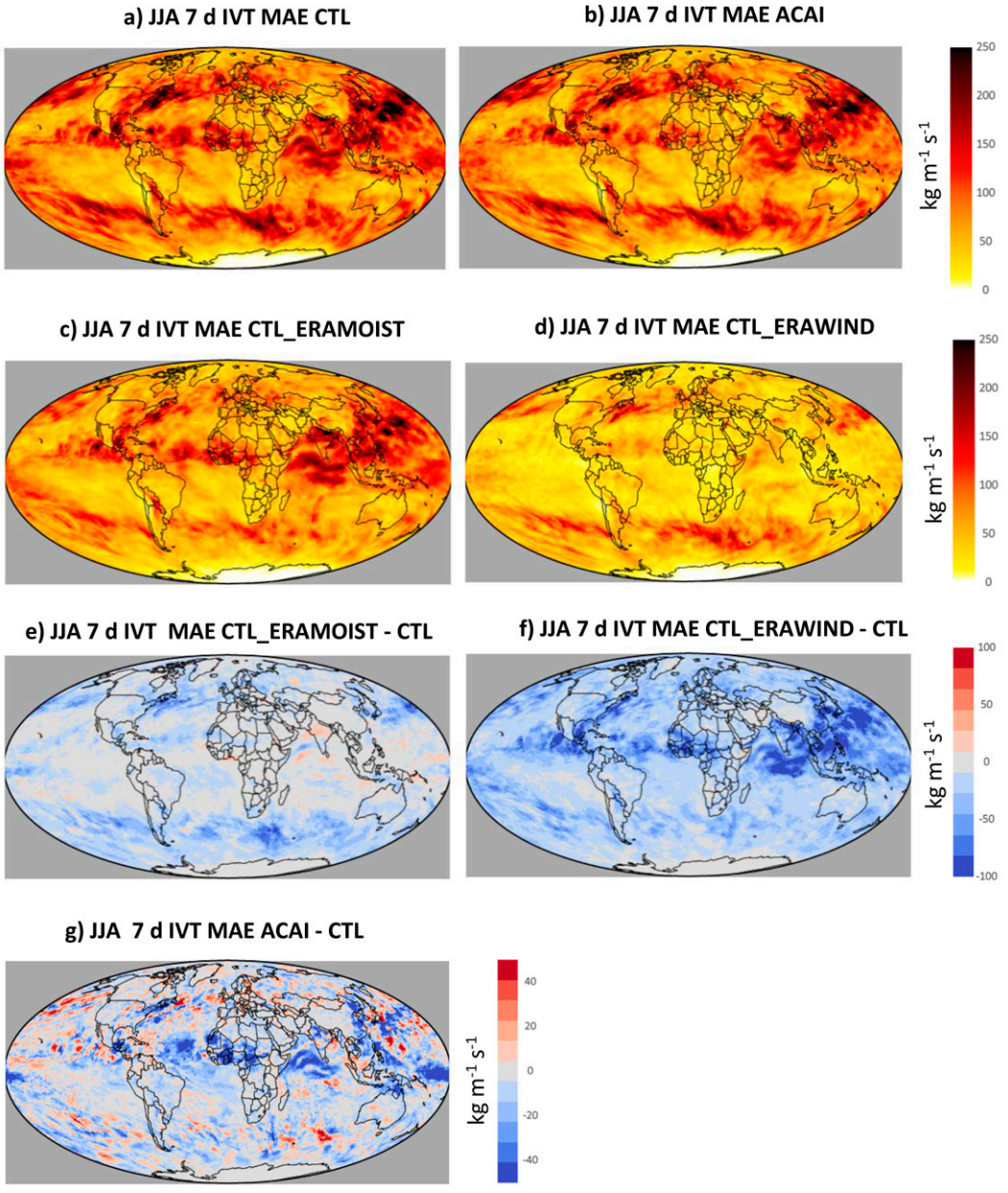

FIG. 10. JJA 7-day IVT mean absolute error (MAE; kg m^{-1} s^{-1}) for (a) CTL, (b) ACAI, (c) CTL_ERAMOIST, (d) CTL_ERAWIND, (e) CTL_ERAMOIST − CTL, (f) CTL_ERAWIND − CTL, and (g) ACAI − CTL.

global coupled system, decomposing the separate contributions of moisture and winds to interpret the results. Overall, ACAI is effective at reducing biases in several, but not all, regions. In a globally averaged sense, ACAI is about twice as effective at reducing TPW bias (by over 30% at forecast day 14), than reducing IVT or 850-hPa wind speed biases (by about 15% at forecast day 14). Locally the reductions in bias may be much larger, such as over the western-central tropical Pacific and northern tropical Africa where ACAI reduces the 14-day JJA IVT biases by as much as 70%. There are also localized regions where ACAI increases the bias, and this may be due to sampling issues (where the bias signal is noisy, such as east of Japan). It may also be due to the fact that for this set of experiments, the analysis increment archive from which the ACAI forcing is derived is a different year from when the forecasts were run, resulting in state-dependent errors in the bias estimate. Biases may be more appropriately defined if ACAI samples a set of analysis increments valid during the months immediately preceding the forecasts. Testing ACAI with a "trailing" training period is currently ongoing. ACAI is most effective where the biases are fairly stable with increasing forecast lead time. The regions associated

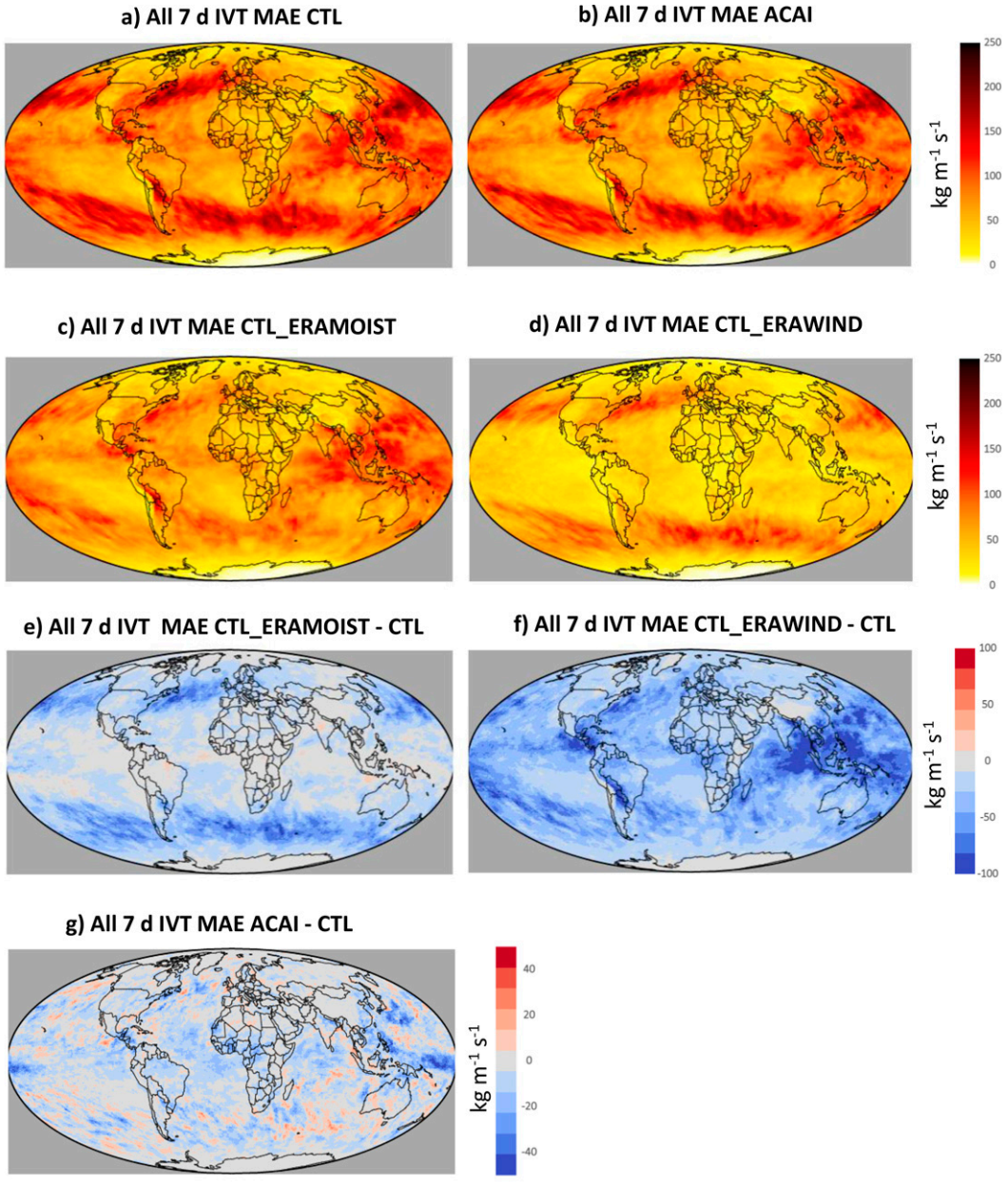

FIG. 11. Year-round 7-day IVT mean absolute error (MAE; kg m^{-1} s^{-1}) for (a) CTL, (b) ACAI, (c) CTL_ERAMOIST, (d) CTL_ERAWIND, (e) CTL_ERAMOIST − CTL, (f) CTL_ERAWIND − CTL, and (g) ACAI − CTL.

with the Indian Monsoon where ACAI actually increases the bias are also regions where the sign and structure of the IVT bias changes with forecast lead time.

Examination of the impact of ACAI on TPW and low-level wind speed indicates that the largest reductions in IVT bias, which occur over the western and central tropical Pacific and over Africa just north of the Gulf of Guinea, are due to reductions in the wind speed biases. ACAI has little impact on the moisture biases in these regions. The increase in IVT bias over the Arabian Sea and India is also driven by an increase in wind speed bias in this region. While the ACAI-induced wind speed bias reductions tend to dominate the IVT bias reductions, there are regions where the reduction in TPW bias plays a dominant role, including the tropical Atlantic and the Sahel.

Recalculating the IVT forecast biases and errors when we substitute in ERA5 analyzed moisture or ERA5 analyzed winds for the forecast fields confirms the dominance of the wind errors over moisture errors in the tropics and subtropics. Using ERA5 winds reduces the global average magnitude of the bias and MAE calculation by about twice as much as using the ERA5 moisture. The dominance of the winds in the bias

calculation is particularly large in the tropics. This explains why the relative reduction in IVT bias by ACAI is closer to the more modest low-level wind bias reductions than the larger moisture bias reductions. There are regions where using either the ERA5 moisture or ERA5 winds increases the bias, revealing areas of compensating errors between the wind and moisture fields.

The extratropical storm tracks are of particular interest, as ARs here have substantial impacts on western North America, western Europe, and other midlatitude regions. In the storm tracks of both hemispheres, wind and moisture errors have comparable contributions to the IVT MAE. This stands in contrast to most of the tropical and subtropical regions, where wind errors dominate IVT errors. The impact of ACAI on IVT is relatively small in these regions and spatially noisy, indicative of sampling issues. Future work should consider the impact on ARs by considering a larger sample size and employing metrics specific to AR forecast skill (e.g., Nardi et al. 2018; DeFlorio et al. 2018, 2019; Cordeira and Ralph 2021).

We have demonstrated utility in using analyzed winds and TPW to understand the dominant components in the IVT error calculations. However, we emphasize that the wind and moisture errors are not independent. For example, errors in tropical rainfall patterns due to the limitations of parameterized convection will drive circulation errors. While our focus has been on IVT biases in this paper, ACAI does reduce the global average MAE by up to 5%, and it also increases the ensemble spread, resulting in improved ensemble calibration. A manuscript focusing on the general performance of ACAI in the Navy ESPC model on a variety of deterministic and probabilistic metrics is in preparation. The results presented here show the promise of ACAI but also show the limitations of the method in regions where the model bias is not relatively stable with forecast time. While decisions on upgrades to operational ensemble systems will be based on a holistic view of the costs and impacts of the proposed changes on an extensive suite of metrics, ideally most shortcomings would be addressed before implementation. In the future, more sophisticated methods of estimating the forecast bias, for example, as a function of forecast lead time, or perhaps including some state dependency, particularly in monsoon regions, would be worth investigating in order to mitigate some of these limitations.

Acknowledgments. We gratefully acknowledge the support of the Chief of Naval Research through the NRL Base Program, PE 0601153N. Computational resources were provided by the Navy Department of Defense Supercomputing Resource Center in Stennis, Mississippi. We thank two anonymous reviewers for insightful and constructive reviews that have helped us improve the manuscript.

Data availability statement. The ERA5 reanalyses are publicly available at https://www.ecmwf.int/en/forecasts/datasets/reanalysis-datasets/era5. The Navy ESPC simulation data have not been released for public access.

REFERENCES

Albano, C. M., M. D. Dettinger, and A. A. Harpold, 2020: Patterns and drivers of atmospheric river precipitation and hydrologic impacts across the western United States. *J. Hydrometeor.*, **21**, 143–159, https://doi.org/10.1175/JHM-D-19-0119.1.

Barton, N., M. Janiga, J. McLay, C. Reynolds, C. Rowley, T. Hogan, and P. Thoppil, 2019: Earth system prediction capability initial operational capability ensemble system. NRL Tech. Memo. NRL/MR/7532-19-9928, 72 pp., https://apps.dtic.mil/sti/citations/AD1111596.

——, and Coauthors, 2021: The Navy's Earth system prediction capability. *Earth Space Sci.*, **8**, e2020EA001199, https://doi.org/10.1029/2020EA001199.

Berner, J., and Coauthors, 2017: Stochastic parameterizations: Toward a new view of weather and climate models. *Bull. Amer. Meteor. Soc.*, **98**, 565–588, https://doi.org/10.1175/BAMS-D-15-00268.1.

Bowler, N. E., and Coauthors, 2017: Inflation and localization tests in the development of an ensemble of 4D-ensemble variational assimilations. *Quart. J. Roy. Meteor. Soc.*, **143**, 1280–1302, https://doi.org/10.1002/qj.3004.

Camargo, S. J., K. A. Emanuel, and A. H. Sobel, 2007: Use of a genesis potential index to diagnose ENSO effects on tropical cyclone genesis. *J. Climate*, **20**, 4819–4834, https://doi.org/10.1175/JCLI4282.1.

Chassignet, E. P., L. T. Smith, G. R. Halliwell, and R. Bleck, 2003: North Atlantic simulations with the HYbrid Coordinate Ocean Model (HYCOM): Impact of the vertical coordinate choice, reference density, and thermobaricity. *J. Phys. Oceanogr.*, **33**, 2504–2526, https://doi.org/10.1175/1520-0485(2003)033<2504:NASWTH>2.0.CO;2.

Cobb, A., L. Delle Monache, F. Cannon, and F. M. Ralph, 2021: Representation of dropsonde-observed atmospheric river conditions in reanalyses. *Geophys. Res. Lett.*, **48**, e2021GL093357, https://doi.org/10.1029/2021GL093357.

Cordeira, J. M., and F. M. Ralph, 2021: A summary of GFS ensemble integrated water vapor transport forecasts and skill along the U.S. West Coast during water years 2017–20. *Wea. Forecasting*, **36**, 361–377, https://doi.org/10.1175/WAF-D-20-0121.1.

Crawford, W., S. Frolov, J. McLay, C. A. Reynolds, N. Barton, B. Ruston, and C. H. Bishop, 2020: Using analysis corrections to address model error in atmospheric forecasts. *Mon. Wea. Rev.*, **148**, 3729–3745, https://doi.org/10.1175/MWR-D-20-0008.1.

Cummings, J. A., and O. M. Smedstad, 2014: Ocean data impacts in global HYCOM. *J. Atmos. Oceanic Technol.*, **31**, 1771–1791, https://doi.org/10.1175/JTECH-D-14-00011.1.

DeFlorio, M. J., D. E. Waliser, B. Guan, D. A. Lavers, F. M. Ralph, and F. Vitart, 2018: Global assessment of atmospheric river prediction skill. *J. Hydrometeor.*, **19**, 409–426, https://doi.org/10.1175/JHM-D-17-0135.1.

——, ——, ——, F. M. Ralph, and F. Vitart, 2019: Global evaluation of atmospheric river subseasonal prediction skill. *Climate Dyn.*, **52**, 3039–3060, https://doi.org/10.1007/s00382-018-4309-x.

Dettinger, M. D., F. M. Ralph, T. Das, P. J. Neiman, and D. Cayan, 2011: Atmospheric rivers, floods, and the water resources of California. *Water*, **3**, 445–478, https://doi.org/10.3390/w3020445.

Gimeno, L., R. Nieto, M. Vazquez, and D. A. Lavers, 2014: Atmospheric rivers: A mini-review. *Front. Earth Sci.*, **2**, 2, https://doi.org/10.3389/feart.2014.00002.

Hersbach, H., and Coauthors, 2020: The ERA5 global reanalysis. *Quart. J. Roy. Meteor. Soc.*, **146**, 1999–2049, https://doi.org/10.1002/qj.3803.

Hogan, T., and Coauthors, 2014: The Navy global environmental model. *Oceanography*, **27**, 116–125, https://doi.org/10.5670/oceanog.2014.73.

Houtekamer, P. L., L. Lefaivre, J. Derome, H. Ritchie, and H. L. Mitchell, 1996: A system simulation approach to ensemble prediction. *Mon. Wea. Rev.*, **124**, 1225–1242, https://doi.org/10.1175/1520-0493(1996)124<1225:ASSATE>2.0.CO;2.

Hunke, E. C., and W. H. Lipscomb, 2015: CICE: The Los Alamos Sea Ice Model documentation and software user's manual, version 4.0. Los Alamos National Laboratory, 72 pp.

Kucukkaraca, E., and M. Fisher, 2006: Use of analysis ensembles in estimating flow-dependent background error variances. *ECMWF Newsletter*, No. 492, ECMWF, Reading, United Kingdom, https://doi.org/10.21957/36n2z0p1p.

Kuhl, D. D., T. E. Rosmond, C. H. Bishop, J. McLay, and N. L. Baker, 2013: Comparison of hybrid ensemble/4DVar and 4DVar within the NAVDAS-AR data assimilation framework. *Mon. Wea. Rev.*, **141**, 2740–2758, https://doi.org/10.1175/MWR-D-12-00182.1.

Lavers, D. A., and G. Villarini, 2013: The nexus between atmospheric rivers and extreme precipitation across Europe. *Geophys. Res. Lett.*, **40**, 3259–3264, https://doi.org/10.1002/grl.50636.

——, R. P. Allan, E. F. Wood, G. Villarini, D. J. Brayshaw, and A. J. Wade, 2011: Winter floods in Britain are connected to atmospheric rivers. *Geophys. Res. Lett.*, **38**, L23803, https://doi.org/10.1029/2011GL049783.

——, M. J. Rodwell, D. S. Richardson, F. M. Ralph, J. D. Doyle, C. A. Reynolds, V. Tallapragada, and F. Pappenberger, 2018: The gauging and modeling of rivers in the sky. *Geophys. Res. Lett.*, **45**, 7828–7834, https://doi.org/10.1029/2018GL079019.

——, and Coauthors, 2020: Forecast errors and uncertainties in atmospheric rivers. *Wea. Forecasting*, **35**, 1447–1458, https://doi.org/10.1175/WAF-D-20-0049.1.

Lawrence, D. M., and P. J. Webster, 2002: The boreal summer intraseasonal oscillation: Relationship between northward and eastward movement of convection. *J. Atmos. Sci.*, **59**, 1593–1606, https://doi.org/10.1175/1520-0469(2002)059<1593:TBSIOR>2.0.CO;2.

Lee, J.-Y., B. Wang, M. C. Wheeler, X. Fu, D. E. Waliser, and I.-S. Kang, 2013: Real-time multivariate indices for the boreal summer intraseasonal oscillation over the Asian summer monsoon region. *Climate Dyn.*, **40**, 493–509, https://doi.org/10.1007/s00382-012-1544-4.

Lélé, M. I., L. M. Leslie, and P. Lamb, 2015: Analysis of low-level atmospheric moisture transport associated with the West African monsoon. *J. Climate*, **28**, 4414–4430, https://doi.org/10.1175/JCLI-D-14-00746.1.

Li, W., and Coauthors, 2019: Evaluating the MJO prediction skill from different configurations of NCEP GEFS extended forecasts. *Climate Dyn.*, **52**, 4923–4936, https://doi.org/10.1007/s00382-018-4423-9.

Metzger, J., and Coauthors, 2014: U.S. Navy operational global ocean and Arctic ice prediction systems. *Oceanography*, **27**, 32–43, https://doi.org/10.5670/oceanog.2014.66.

Meynadier, R., O. Bock, S. Gervois, F. Guichard, J.-L. Redelsperger, A. Agustí-Panareda, and A. Beljaars, 2010: West African monsoon water cycle: 2. Assessment of numerical weather prediction water budgets. *J. Geophys. Res.*, **115**, D19107, https://doi.org/10.1029/2010JD013919.

Mo, K., and R. W. Higgins, 1996: Large-scale atmospheric moisture transport as evaluated in the NCEP/NCAR and the NASA/DAO reanalyses. *J. Climate*, **9**, 1531–1545, https://doi.org/10.1175/1520-0442(1996)009<1531:LSAMTA>2.0.CO;2.

Nardi, K. M., E. A. Barnes, and F. M. Ralph, 2018: Assessment of numerical weather prediction model reforecasts of the occurrence, intensity, and location of atmospheric rivers along the west coast of North America. *Mon. Wea. Rev.*, **146**, 3343–3362, https://doi.org/10.1175/MWR-D-18-0060.1.

Neiman, P. J., L. J. Schick, F. M. Ralph, M. Hughes, and G. A. Wick, 2011: Flooding in western Washington: The connection to atmospheric rivers. *J. Hydrometeor.*, **12**, 1337–1358, https://doi.org/10.1175/2011JHM1358.1.

Newman, M., G. N. Kiladis, K. M. Weickmann, F. M. Ralph, and D. Sardeshmukh, 2012: Relative contributions of synoptic and low-frequency eddies to time-mean atmospheric moisture transport, including the role of atmospheric rivers. *J. Climate*, **25**, 7341–7361, https://doi.org/10.1175/JCLI-D-11-00665.1.

Peixoto, J. P., and A. H. Oort, 1992: *Physics of Climate*. American Institute of Physics, 520 pp.

Piccolo, C., and M. J. P. Cullen, 2016: Ensemble data assimilation using a unified representation of model error. *Mon. Wea. Rev.*, **144**, 213–224, https://doi.org/10.1175/MWR-D-15-0270.1.

——, ——, W. J. Tennant, and A. T. Semple, 2019: Comparison of different representations of model error in ensemble forecasts. *Quart. J. Roy. Meteor. Soc.*, **145**, 15–27, https://doi.org/10.1002/qj.3348.

Ralph, F. M., P. J. Neiman, G. A. Wick, S. I. Gutman, M. D. Dettinger, D. R. Cayan, and A. B. White, 2006: Flooding on California's Russian River: Role of atmospheric rivers. *Geophys. Res. Lett.*, **33**, L13801, https://doi.org/10.1029/2006GL026689.

——, and Coauthors, 2017: Dropsonde observations of total integrated water vapor transport within North Pacific atmospheric rivers. *J. Hydrometeor.*, **18**, 2577–2596, https://doi.org/10.1175/JHM-D-17-0036.1.

——, J. J. Rutz, J. M. Cordeira, M. Dettinger, M. Anderson, D. Reynolds, L. J. Schick, and C. Smallcomb, 2019: A scale to characterize the strength and impact of atmosphere rivers. *Bull. Amer. Meteor. Soc.*, **100**, 269–289, https://doi.org/10.1175/BAMS-D-18-0023.1.

——, and Coauthors, 2020: West Coast forecast challenges and development of atmospheric river reconnaissance. *Bull. Amer. Meteor. Soc.*, **101**, E1357–E1377, https://doi.org/10.1175/BAMS-D-19-0183.1.

Ramos, A. M., R. M. Trigo, M. L. R. Liberato, and T. Ricardo, 2015: Daily precipitation extreme events in the Iberian Peninsula and its association with atmospheric rivers. *J. Hydrometeor.*, **16**, 579–597, https://doi.org/10.1175/JHM-D-14-0103.1.

Redelsperger, J. L., C. D. Thorncroft, A. Diedhiou, T. Lebel, D. J. Parker, and J. Polcher, 2006: African Monsoon Multidisciplinary Analysis: An international research project and field campaign. *Bull. Amer. Meteor. Soc.*, **87**, 1739–1746, https://doi.org/10.1175/BAMS-87-12-1739.

Rosmond, T., and L. Xu, 2006: Development of NAVDAS-AR: Non-linear formulation and outer loop tests. *Tellus*, **58A**, 45–58, https://doi.org/10.1111/j.1600-0870.2006.00148.x.

Ruston, B., C. A. Reynolds, T. Whitcomb, M. Janiga, E. J. Metzger, J. Shriver, M. Cobb, and J. Feldmeier, 2019: Earth system prediction capability initial operational capability

deterministic system. NRL Memo. NRL/MR/7531-19-9935, 124 pp., https://apps.dtic.mil/sti/citations/AD1090615.

Rutz, J. J., and Coauthors, 2019: The Atmospheric River Tracking Method Intercomparison Project (ARTMIP): Quantifying uncertainties in atmospheric river climatology. *J. Geophys. Res. Atmos.*, **124**, 13 777–13 802, https://doi.org/10.1029/2019JD030936.

Sahana, A. S., A. Pathak, M. K. Roxy, and S. Ghosh, 2019: Understanding the role of moisture transport on the dry bias in Indian Monsoon simulations by CFSv2. *Climate Dyn.*, **52**, 637–651, https://doi.org/10.1007/s00382-018-4154-y.

Shaw, T. A., and O. Pauluis, 2012: Tropical and subtropical meridional latent heat transport by disturbances to the zonal mean and their role in the general circulation. *J. Atmos. Sci.*, **69**, 1872–1889, https://doi.org/10.1175/JAS-D-11-0236.1.

Shields, C. A., and Coauthors, 2018: Atmospheric River Tracking Method Intercomparison Project (ARTMIP): Project goals and experimental design. *Geosci. Model Dev.*, **11**, 2455–2474, https://doi.org/10.5194/gmd-11-2455-2018.

Sohn, B. J., and S.-C. Park, 2010: Strengthened tropical circulations in past three decades inferred from water vapor transport. *J. Geophys. Res.*, **115**, D15112, https://doi.org/10.1029/2009JD013713.

Theurich, G., and Coauthors, 2016: The Earth system prediction suite: Toward a coordinated U.S. modeling capability. *Bull. Amer. Meteor. Soc.*, **97**, 1229–1247, https://doi.org/10.1175/BAMS-D-14-00164.1.

Thorncroft, C. D., H. Nguyen, C. Zhang, and P. Peyrille, 2011: Annual cyclone of the West African monsoon: Regional circulations and associated water vapor transport. *Quart. J. Roy. Meteor. Soc.*, **137**, 129–147, https://doi.org/10.1002/qj.728.

Trenberth, K. E., J. T. Fasullo, and J. Mackaro, 2011: Atmospheric moisture transports from ocean to land and global energy flows in reanalyses. *J. Climate*, **24**, 4907–4924, https://doi.org/10.1175/2011JCLI4171.1.

Viale, M., R. Valenzuela, R. D. Garreaud, and F. M. Ralph, 2018: Impacts of atmospheric rivers on precipitation in southern South America. *J. Hydrometeor.*, **19**, 1671–1687, https://doi.org/10.1175/JHM-D-18-0006.1.

Wang, Z., G. Li, and S. Yang, 2018: Origin of Indian summer monsoon rainfall biases in CMIP5 multimodel ensemble. *Climate Dyn.*, **51**, 755–768, https://doi.org/10.1007/s00382-017-3953-x.

Weisheimer, A., S. Corti, T. N. Palmer, and F. Vitart, 2014: Addressing model error through atmospheric stochastic physical parameterizations: Impact on the coupled ECMWF seasonal forecasting system. *Philos. Trans. Roy. Soc. London*, **A372**, 2013029, https://doi.org/10.1098/rsta.2013.0290.

Xue, Y., and Coauthors, 2010: Intercomparison and analyses of the climatology of West African Monsoon in the West African Monsoon Modeling and Evaluation project (WAMME) first model intercomparison experiment. *Climate Dyn.*, **35**, 3–27, https://doi.org/10.1007/s00382-010-0778-2.

Xie, S., H. Ma, J. S. Boyle, S. A. Klein, and Y. Zhang, 2012: On the correspondence between short- and long-time-scale systematic errors in CAM4/CAM5 for the year of tropical convection. *J. Climate*, **25**, 7937–7955, https://doi.org/10.1175/JCLI-D-12-00134.1.

Zhu, Y., and R. E. Newell, 1998: A proposed algorithm for moisture fluxes from atmospheric rivers. *Mon. Wea. Rev.*, **126**, 725–735, https://doi.org/10.1175/1520-0493(1998)126<0725:APAFMF>2.0.CO;2.